J. Fluid Mech. (1991), *vol.* 225, *pp.* 241–270
Printed in Great Britain

Two-layer geostrophic vortex dynamics. Part 2. Alignment and two-layer V-states

By L. M. POLVANI†
Department of Mathematics, Room 2-339, Massachusetts Institute of Technology, Cambridge, MA 02139, USA

(Received 13 June 1989 and in revised form 17 September 1990)

The process of *alignment*, a new fundamental interaction between vortices in a stratified and rapidly rotating fluid, is defined and studied in detail in the context of the two-layer quasi-geostrophic model. Alignment occurs when two vortices in different density layers coalesce by reducing their horizontal separation. It is found that only vortices whose radii are comparable with or larger than the Rossby deformation radius can align. In the same way as the merger process (in a single two-dimensional layer) is related to the reverse energy cascade of two-dimensional turbulence, geostrophic potential vorticity alignment is related the barotropic-to-baroclinic energy cascade of geostrophic turbulence in two layers. It is also shown how alignment is intimately connected with the existence of two-layer doubly connected geostrophic potential vorticity equilibria (V-states), for which the analysis of the geometry of the stream function in the corotating frame is found to be a crucial diagnostic. The finite-area analogues of the *hetons* of Hogg & Stommel (1985) are also determined: they consist of a propagating pair of opposite-signed potential vorticity patches located in different layers.

1. Introduction

In a companion paper (Polvani, Zabusky & Flierl 1989*a*, hereinafter referred to as 'the first paper') we have presented the results of our study of the dynamics of quasi-geostrophic vortices in a two-layer model for configurations in which the geostrophic potential vorticity in the lower layer is identically zero. The objective was to investigate the effect of the presence of an active lower layer on the dynamics of vortices in the upper layer. Most of the attention was dedicated to the process of vortex *merger*, which is now recognized to be the fundamental interaction through which long-lived isolated strong coherent vortices are generated in two-dimensional turbulent fields (McWilliams 1984; Babiano *et al.* 1986; Benzi, Paternello & Santangelo 1988).

In the first paper, the presence of a finite radius of deformation L_R was found to inhibit merger for vortices of radius comparable with L_R when the lower layer is deep. The critical merger distances as functions of L_R were shown to be closely related to the limiting shapes of same-sign vortex pair equilibria (V-states). It was also determined that the equivalent barotropic model is a singular limit of the two-layer model (as the lower layer becomes infinitely deep), its dynamics exhibiting a strong suppression of filamentation and axisymmetrization for scales of order L_R and larger.

† Present address: Department of Applied Physics, Columbia University, New York, NY 10027, USA.

For more details we refer the reader to the first paper (see also Polvani, Flierl & Zabusky 1989*b*).

In this second paper we turn our attention to situations in which the geostrophic potential vorticity is non-zero in both layers. Unfortunately our knowledge of stratified geostrophic turbulence is less advanced than for two-dimensional turbulence. The original observation of Charney (1971) that the geostrophic form of the potential vorticity is isomorphic to the two-dimensional vorticity, thereby implying a k^{-3} spectral law, reverse energy and forward enstrophy cascades, and equipartition between kinetic and potential energy, has been generally confirmed by Herring (1980), who used a statistical closure model and, more recently, by the numerical simulations of Hua & Haidvogel (1986). (Here k is the magnitude of the three-dimensional wavenumber, with the vertical coordinate rescaled by the ratio N/f of the Brunt–Väisälä frequency to the Coriolis parameter.)

A number of other investigators have instead concentrated on models with low vertical resolution, and in particular on the two-layer model (see Rhines 1979, for a review). Among the important results that have emerged from these studies we mention the presence of a 'red' cascade of the barotropic energy to the large scales (analogous to the two-dimensional case) and a baroclinic forward cascade to the smaller scales (a manifestation of baroclinic instability). Moreover, the intermodal barotropic–baroclinic interactions have been shown to lead to an energy transfer from baroclinic to barotropic modes, and to occur preferentially on scales close to the deformation radius.

The first suggestion of the presence of isolated and coherent structures in stratified quasi-geostrophic turbulence was reported by Hua & Haidvogel (1986), and a clear picture of their emergence in the decaying case has recently been presented by McWilliams (1989) with a simulation at unprecedently high resolution. In particular, McWilliams reports how the coherent vortices of stratified geostrophic turbulence seem to be mostly elongated in the vertical direction and horizontally axisymmetric.

Motivated by these results, we start in §2 by defining and studying in detail, within the framework of the two-layer model, a new fundamental process which, following McWilliams' description, we have termed *vortex alignment*: it is the stratified counterpart of the merger process, and we believe it to be responsible for the predominantly columnar (i.e. vertically untilted) character of stratified geostrophic vortices. The fundamental nature of alignment resides in that it is related to the baroclinic-to-barotropic energy cascade (Rhines 1979), much as merger is related to the well-known reverse energy cascade of two-dimensional turbulence (Kraichnan & Montgomery 1980); the energy conversion is quantified in §3. The connection between alignment and the existence (or rather the absence) of geostrophic potential vorticity equilibria (V-states) is studied in §4, and their rich and complicated structure is carefully examined in §5, where the principal diagnostic tool is shown to be the analysis of the geometry of corotating stream functions. Finally, we present in §6 the finite-area analogues of the self-propagating geostrophic point-vortex pairs called 'hetons' by Hogg & Stommel (1985).

2. Alignment in the two-layer model

The quasi-geostrophic two-layer model is the simplest system that exhibits the properties of both rotation and stratification, and we have adopted it in this investigation as a physical system ideally suited for a detailed study of fundamental processes in the dynamics of stratified rotating vorticity fields. The system is

composed of two equal layers of constant density in which the flow is two-dimensional and given by a stream function $\psi_i (i = 1, 2)$ which is related to the dynamically conserved quantity, the geostrophic potential vorticity Π_i, through the relation

$$\Pi_i = \nabla^2 \psi_i + \gamma^2 (\psi_j - \psi_i) \quad \text{with} \quad i = 1, 2, \quad j = 3 - i, \tag{1}$$

where the non-dimensional parameter γ corresponds to the ratio of the lengthscale of the motion (here the radius of the vortex patches) to the radius of deformation. To reduce the computational task we have confined our study, in this second paper, to the case of two layers of equal depth in the absence of motion (for more details on the two-layer model, we refer the reader to the first paper and references therein).

The alignment process is studied by considering the evolution of two initially circular vortex patches, i.e. two regions of uniform Π, one in each layer. We let $\Pi = 1$ inside the vortices and zero everywhere outside and, without loss of generality, we choose the radius of the vortices to be 1 and their horizontal separation d_c. The choice of a uniform Π within the vortices allows us to determine the evolution of the system uniquely from the position of the contours enclosing the non-zero geostrophic potential vorticity: the method of contour dynamics and its implementation for the two-layer model have been described in detail in the first paper. However, the numerical algorithm with which the following results were obtained differs considerably from the one used there.

The computations presented here were performed with an algorithm based on Dritschel's (1988*a*) contour surgery for the two-dimensional Euler equations, appropriately modified for the two-layer model. Contour surgery not only uses a higher-order interpolation scheme for the contours, but also allows for automatic topological reconnections. Because the situation of interest in our problem is such that the geostrophic potential vorticity in one layer is a symmetric reflection about the origin of that in the opposite layer, much computational time can be saved and accuracy obtained by computing the evolution of the contours in a single layer, and reflecting about the origin to obtain the contours in the other layer. In general, for the results presented in this section, the area is numerically conserved to better than 1 part in 10^4 at the end of each run, with the exception of those instances in which a very large amount of filamentation occurs, in which case area conservation is only the order of 0.5%.

By analogy with the merger problem we would like to be able to say that two vortices align when the horizontal distance between them decreases. The novelty with respect to merger is that, because they are located in different layers, we have the possibility, in the alignment problem, of starting the two vortices with a large amount of overlap; it is therefore crucial to have a precise quantitative definition of alignment. The natural choice is to make use of the intercentroid distance (i.e. the horizontal distance between the two centres of vorticity) as the relevant diagnostic quantity.

Two scenarios are possible: when the intercentroid distance decreases (within a time of the order of the rotation period t_c of the vortices about their common centroid) to an average value lower than the initial one, we deem that alignment has occurred. Alternatively, when the vortices do not align, the intercentroid distance merely oscillates† with time around a constant value. We now present a number of

† The question of whether this oscillation is actually periodic is not addressed here since we are only interested in vortex interactions on times of order t_c, and vortex encounters rarely last much longer in turbulent geostrophic vorticity fields. We note that the question of exact recurrence has not been investigated in detail even for the merger problem in two dimensions.

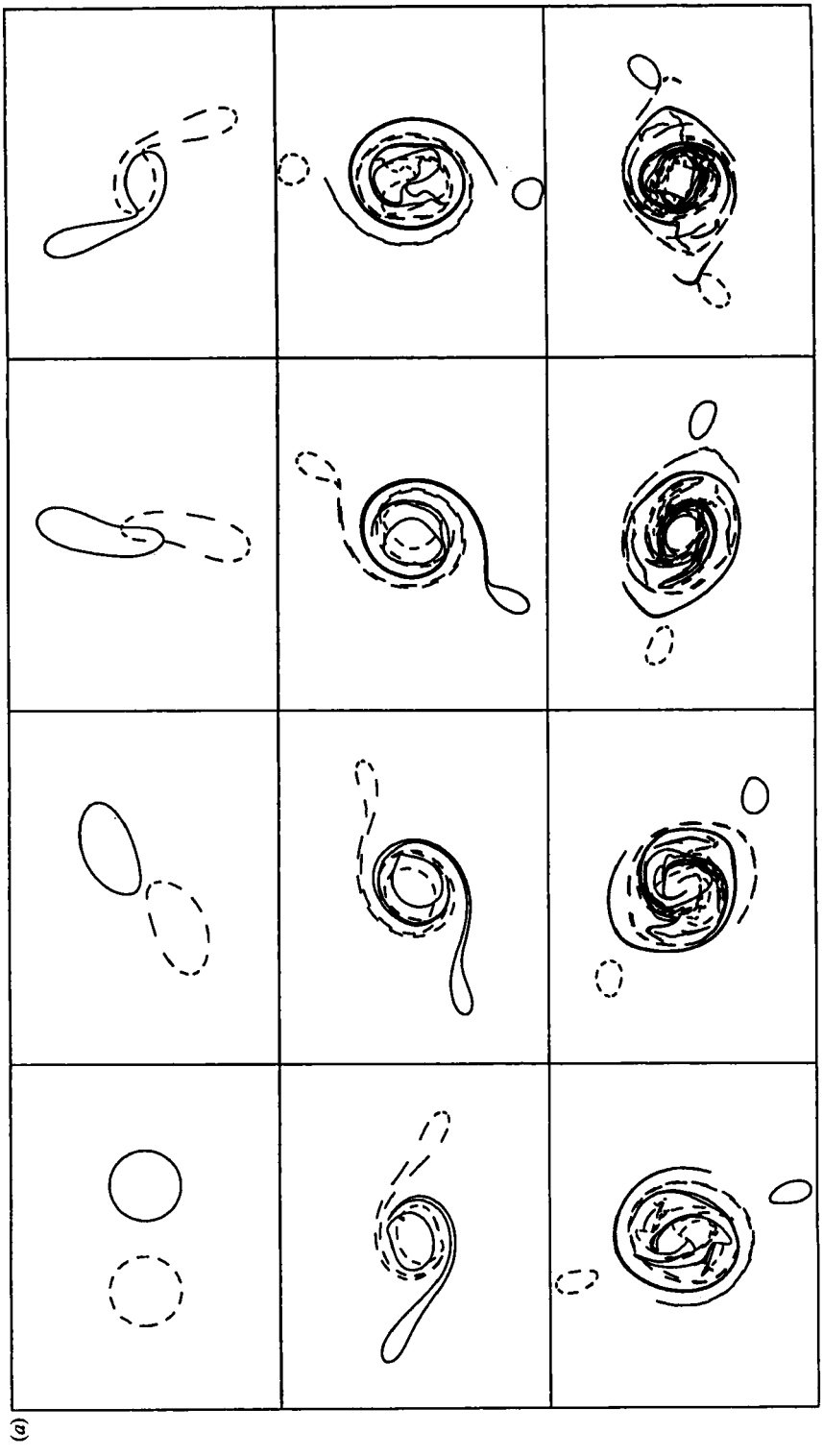

FIGURE 1 (*a*). For caption see facing page.

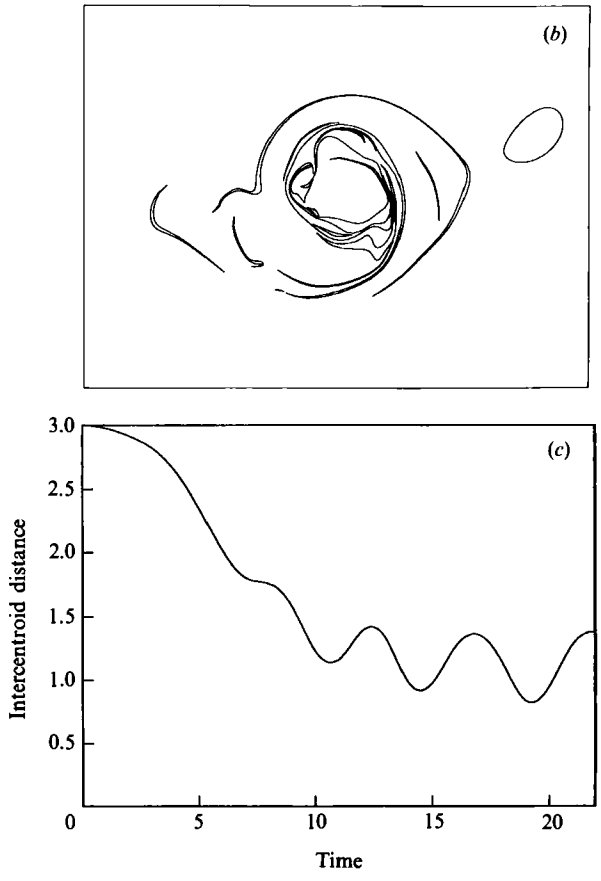

FIGURE 1. (*a*) Alignment for $d_c = 3.0$ and $\gamma = 2.0$. Time advances to the right and downwards. The frames shown are $t = 0, 2, 4, \ldots$. The solid (dashed) contours are in the upper (lower) layer. (*b*) The geostrophic potential vorticity in the upper layer at $t = 22$ for the run in (*a*). (*c*) The intercentroid distance as a function of time for the run in (*a*).

examples that illustrate the rich phenomenology of the alignment problem in the two-dimensional (γ, d_c) parameter space.

In figure 1 (*a*) we show the evolution of two circular vortices, one in each layer, initially separated by a distance $d_c = 3.0$ at $\gamma = 2.0$ (i.e. with a radius twice the deformation radius). The vortex patches, initially well separated, behave as if attracting each other, and eventually a large portion of each vortex is torn away. The final configuration shows that the vorticity has been rearranged so as to be composed of two 'satellite' vortices, one in each layer, rotating about a central barotropic vortex. An expanded view of the vorticity field in the upper layer for the last frame is given in figure 1 (*b*); the vorticity has been split into two main parts, an outer vortex (cf. the rightmost part of figure 1 *b*) and an inner one which is interacting strongly with its counterpart in the lower layer and is surrounded by many filaments. The intercentroid distance as a function of time is plotted in figure 1 (*c*); it drops to approximately $\frac{1}{3}$ of its initial value as alignment takes place, and eventually oscillates around that level.

By reducing the value of γ, which amounts to uncoupling the layers or, alternatively, increasing the Rossby deformation radius of the system, alignment can

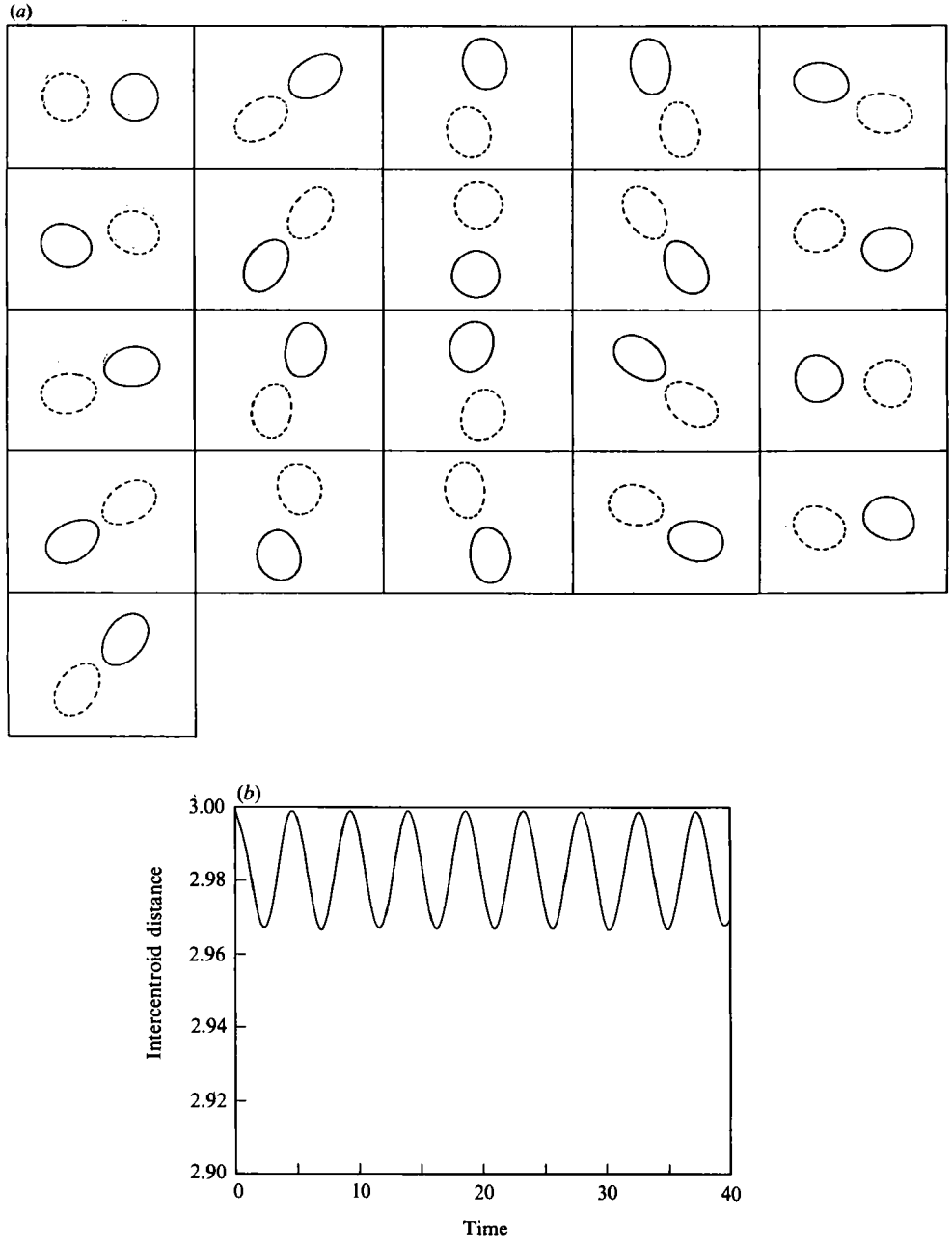

FIGURE 2. (*a*) Same as figure 1 (*a*) but for $\gamma = 1.0$. The frames are shown at $t = 0, 2, 4, \ldots$. (*b*) The intercentroid distance as a function of time for the run in (*a*).

be suppressed. We illustrate this in figure 2 (*a*), where the evolution of two vortices placed at the same distance apart as the previous run, but at $\gamma = 1$, is shown. In this case the vortices simply rotate around one another and their intercentroid distance, plotted in figure 2 (*b*), oscillates with time.

As one would expect, alignment is recovered at the same value of $\gamma = 1$ by approaching the vortices to each other, as is shown in figure 3 (*a*) for the case

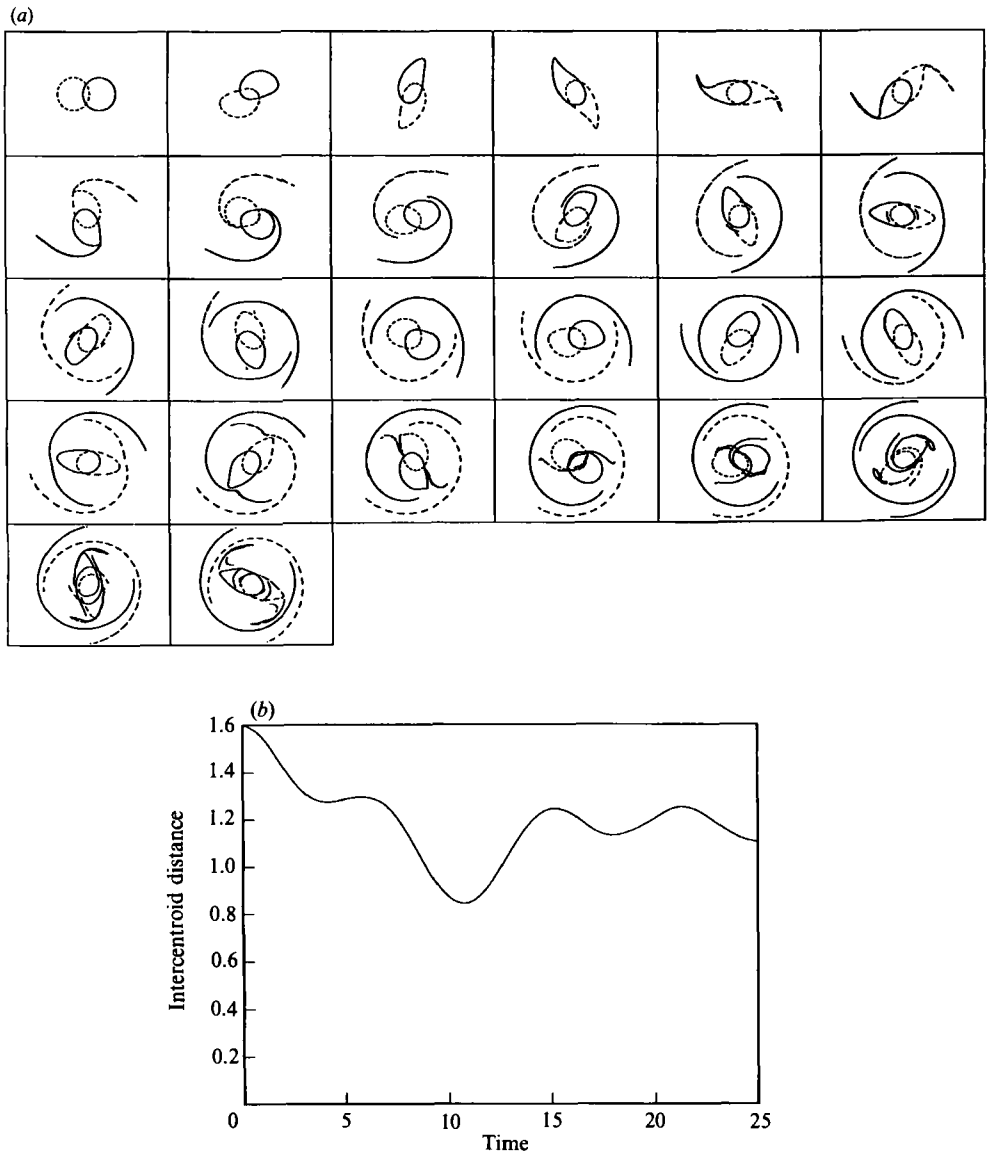

FIGURE 3. (*a*) Alignment for $d_c = 1.6$ and $\gamma = 1.0$. Time advances to the right and downwards. The frames are shown at $t = 0, 1, 2, 3, \ldots$. (*b*) The intercentroid distance as a function of time for the run in (*a*).

$d_c = 1.6$. In this case only a thin filament is initially shed by the vortices, and the intercentroid distance (plotted in figure 3*b*) decreases by a relatively small amount.

If the vortices are now placed even closer together, at the same value of $\gamma = 1$, the first counter-intuitive result is encountered. The case $d_c = 0.4$ (see figure 4*a*) shows no alignment taking place, although the two vortices are initially almost entirely overlapping; the intercentroid distance, shown in figure 4 (*b*), undergoes quite regular oscillations, similar to those in figure 2 (*b*) for a much greater initial separation. From our knowledge of the merger process, one would have expected that starting the vortices at a smaller distance apart for the same value of γ would lead to alignment.

For the same small initial distance $d_c = 0.4$ we find that alignment occurs when the

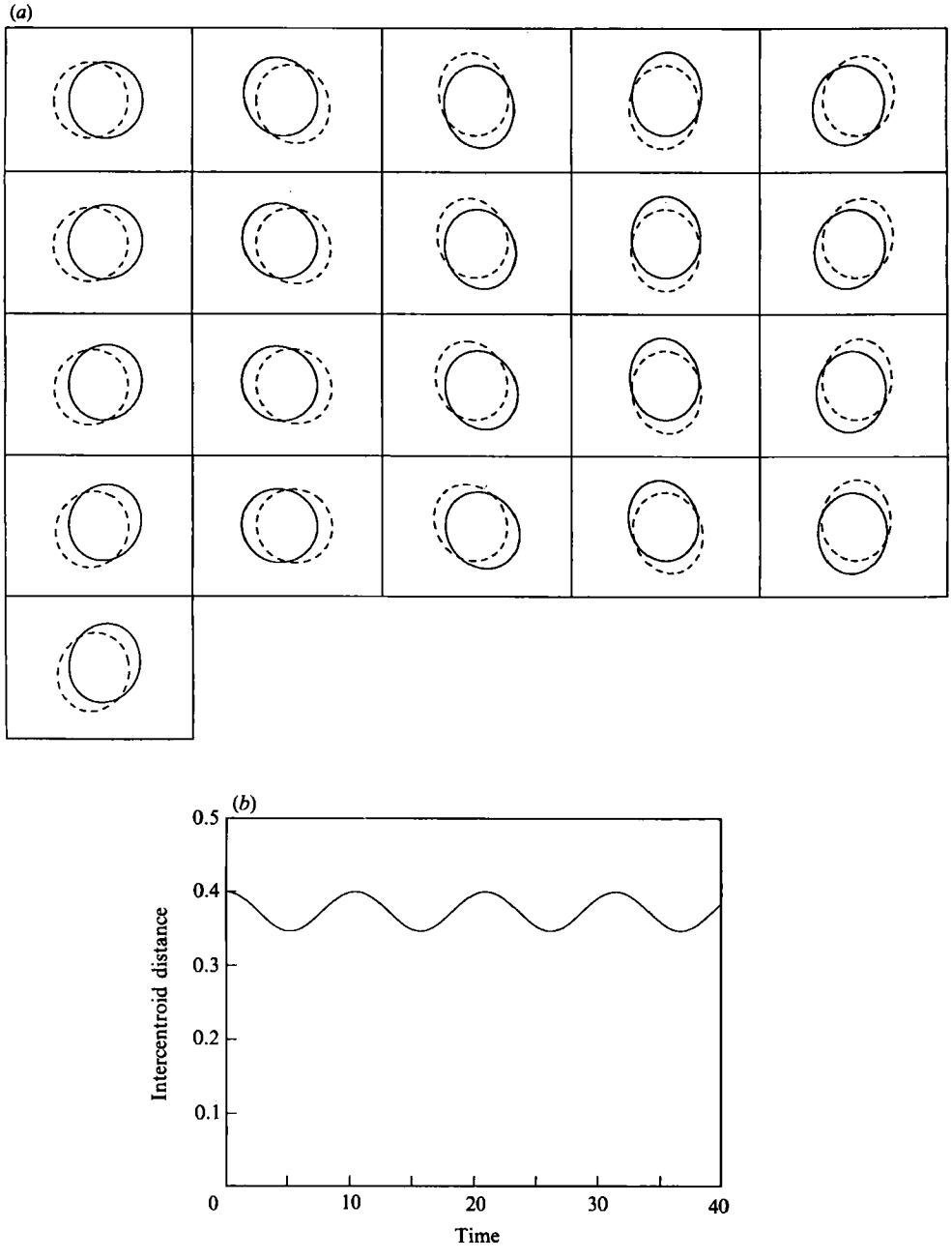

FIGURE 4. (a) Same as figure 2(a) but for $d_c = 0.4$. The frames are shown at $t = 0, 2, 4, \ldots$. (b) The intercentroid distance as a function of time for the run in (a).

vortices are made larger with respect to L_R, i.e. at higher γ. In figure 5(a) an example at $\gamma = 5.0$ is presented. Note that only very thin filaments are shed around the vortices and they are reminiscent of the ones observed by Dritschel (1988*b*).

At this large value of γ, the two layers are very strongly coupled, and the fluid tends to behave as if the vortices were simultaneously present in both layers. We illustrate this with a final example, shown in figure 6, for $d_c = 2.2$ and $\gamma = 5.0$, where

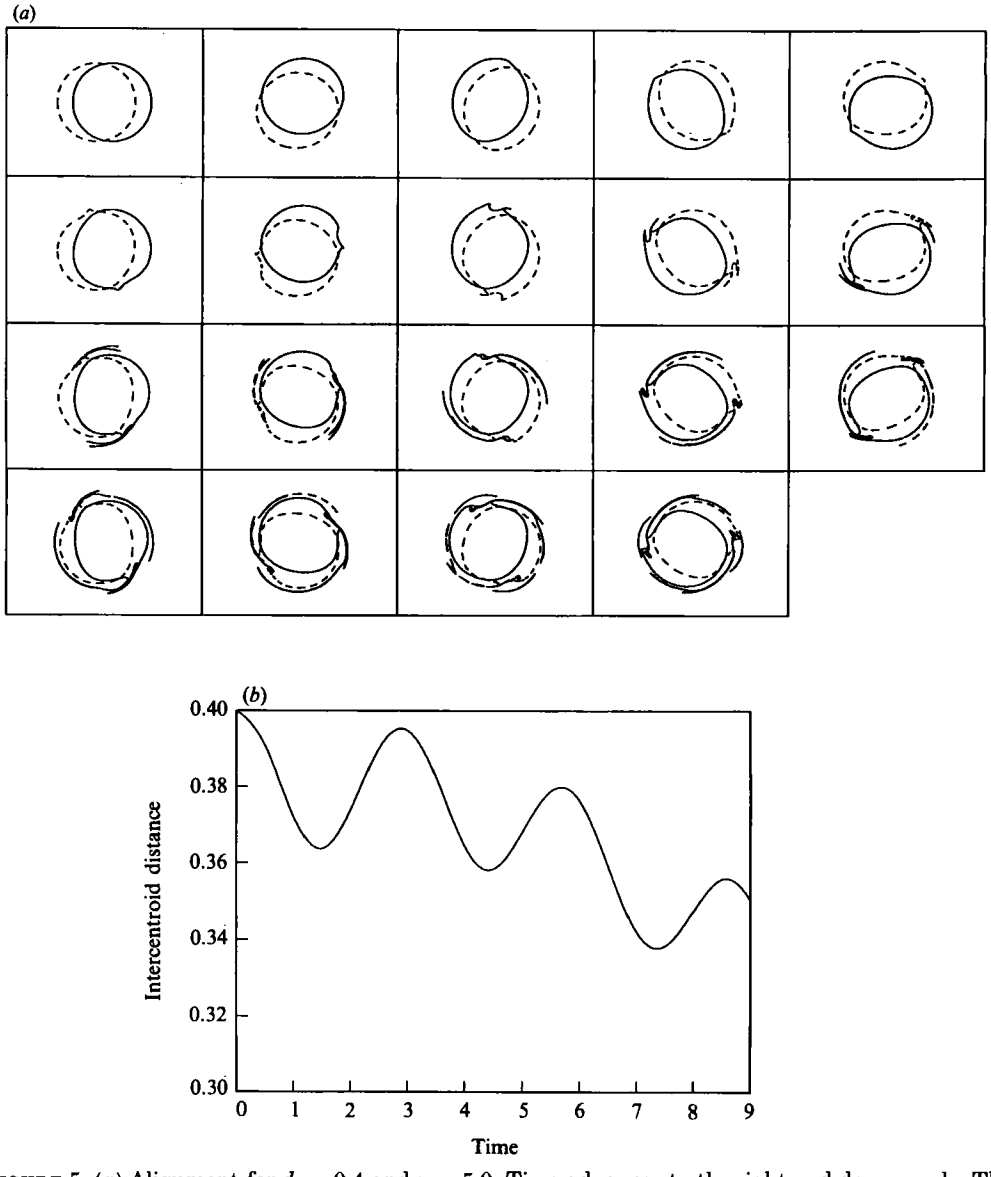

FIGURE 5. (*a*) Alignment for $d_c = 0.4$ and $\gamma = 5.0$. Time advances to the right and downwards. The frames are shown at $t = 0, 1, 2, 3, \ldots$. (*b*) The intercentroid distance as a function of time for the run in (*a*).

the vortices are initialized in a non-overlapping configuration. It is fascinating to observe how similar this alignment is to a merger, in as much as very little overlap between the vortices takes place, at least for the early stages.

The results of our numerical experiments for the alignment problem in the two-layer quasi-geostrophic model are summarized in figure 7. Crosses (respectively circles) represent locations where alignment (no alignment) is found; the line separating the two regions was drawn in by hand. Alignment occurs only for sufficiently large γ, namely for vortices sufficiently large with respect to L_R, and the smallest value of γ for which alignment is possible is found to be very close to 1.

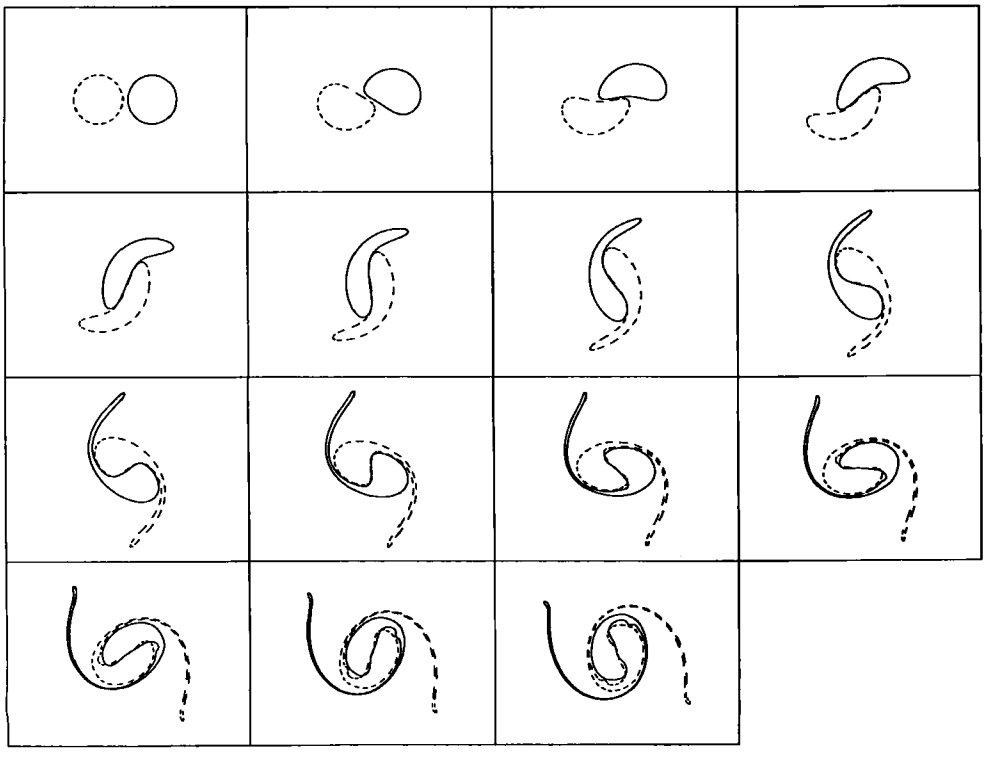

FIGURE 6. Alignment for $d_c = 2.2$ and $\gamma = 5.0$. Time advances to the right and downwards. The frames are shown at $t = 0, 0.5, 1.0, 1.5, \ldots$. The two vortices are located in different layers.

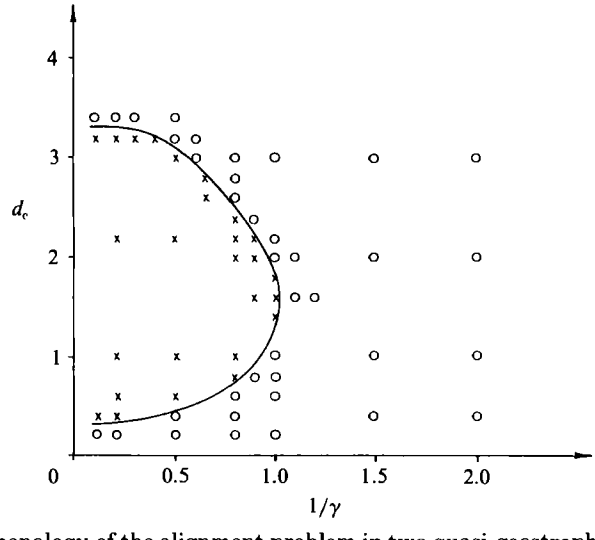

FIGURE 7. Phenomenology of the alignment problem in two quasi-geostrophic layers of equal depth in the (γ, d_c) parameter space. Crosses indicated alignment, and circles no-alignment.

The higher branch of the curve for the critical alignment distance is easily understood in a way analogous to the merger problem: two vortices must be sufficiently close to 'feel each other' and align. Note that in the limit $\gamma \gg 1$ the curve tends to the critical value $d_c \approx 3.3$: the Euler value is recovered in that limit because

the Green function becomes purely logarithmic as $\gamma \to \infty$ (refer to equation (4) of the first paper).

The lower part of the curve is not entirely surprising in view of the recent results on the stability of geostrophic vortices. Flierl (1988) has shown that a barotropic two-layer circular geostrophic potential vorticity patch is stable to $m = 1$ baroclinic disturbances; thus we expect the alignment curve not to intersect the $d_c = 0$ axis. Here m represents the azimuthal wavenumber of a linear normal mode perturbation. Recall that an $m = 1$ baroclinic mode corresponds to a simple displacement of the centres in opposite directions in the two layers. The results of figure 7 suggest that barotropic circular vortices are actually nonlinearly unstable to $m = 1$ baroclinic perturbations of sufficiently large amplitude.

3. Energy conversions in the alignment process

In order to study energy conversions in the alignment problem, we have used a pseudospectral algorithm for integrating the two-layer quasi-geostrophic equations. There are two reasons for doing this. First, energy calculations are very inefficiently done with contour dynamics/surgery since the expressions needed to compute the energies are not easily formulated in terms of contour integrals. Second, and more importantly, we want to show that the results just presented are robust, in the sense that they do not rely in an essential way on the geostrophic potential vorticity field being piecewise uniform.

The computations presented in this section were obtained with a doubly periodic dealiased 128×128 pseudospectral code. Some hyperviscosity (νk^{16}) is necessary to keep the enstrophy bounded in the small scales. However, the dissipation ν is chosen to be sufficiently small that only approximately 0.5% of the total energy is lost at the end of each run. Thus the dynamics of these vortices can be considered, at least for the larger scales, virtually inviscid. As in the previous section, we initialize the fields with two circular patches of uniform identical geostrophic potential vorticity, one in each layer. A small amount of smoothing is necessary near the circular boundaries to avoid Gibbs phenomena due to an infinitely steep gradient.

To separate the baroclinic and barotropic components of the energy, it is convenient to write them in terms of the barotropic and baroclinic stream functions, ψ_T and ψ_C respectively, defined by

$$\psi_T = \tfrac{1}{2}(\psi_1 + \psi_2), \quad \psi_C = \tfrac{1}{2}(\psi_1 - \psi_2), \tag{2}$$

for two layers of equal depth in the absence of motion. The total energy E of the system can then be expressed as a sum of two parts, a barotropic one defined by

$$E_T = \frac{1}{2}\int\int |\nabla \psi_T|^2 \, dA, \tag{3}$$

which is purely kinetic in character, and a baroclinic part which is composed of a kinetic component as well as a potential energy term:

$$E_C = \frac{1}{2}\int\int [|\nabla \psi_C|^2 + 2\gamma^2 \psi_C^2] \, dA. \tag{4}$$

In an inviscid system the total energy $E = E_T + E_C$ is conserved. We now show how energy is converted from E_C to E_T when alignment takes place.

Consider first the alignment presented in figure 8(*a*) for $d_c = 3.0$ and $\gamma = 2.0$; these

(*a*)

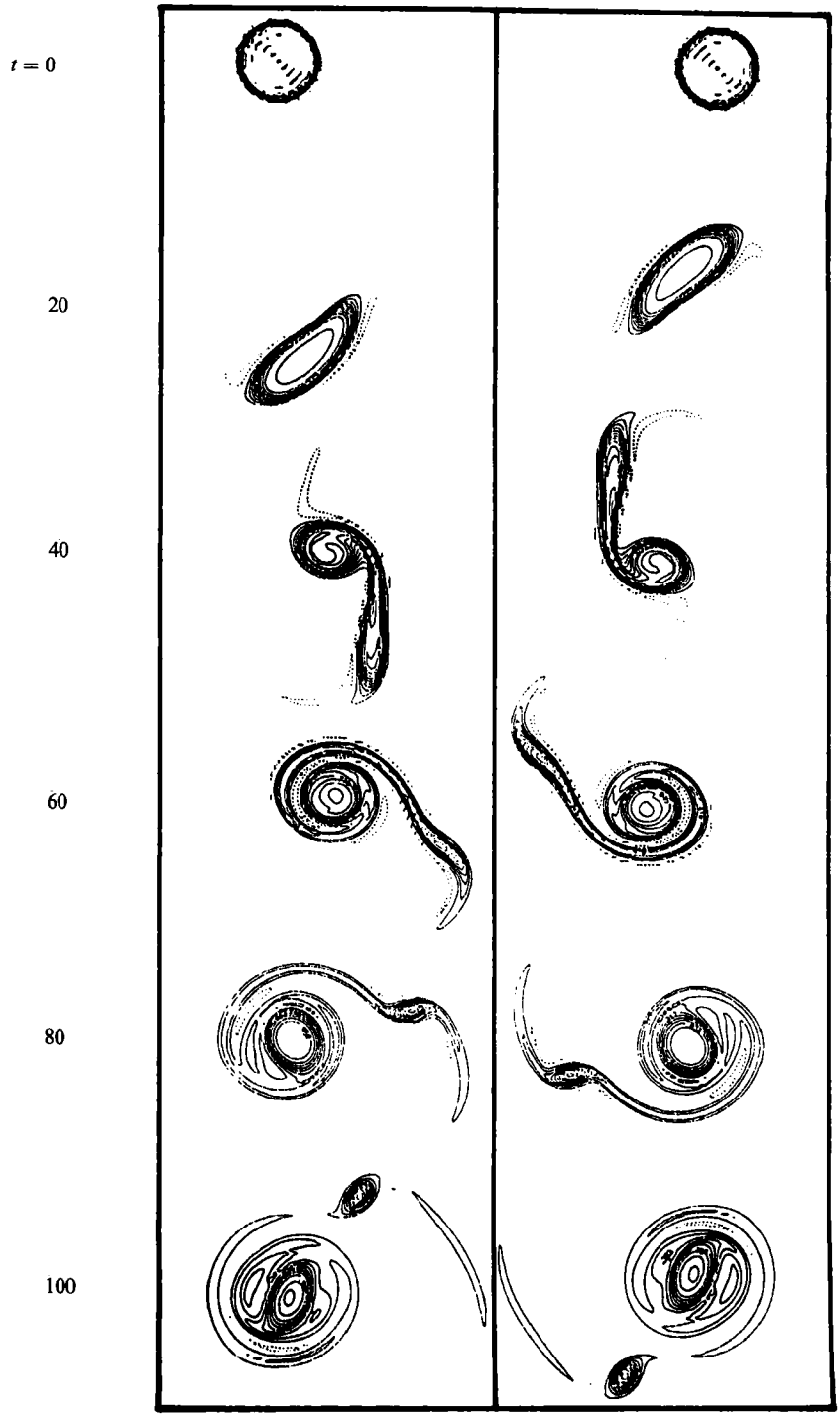

FIGURE 8(*a*). For caption see facing page.

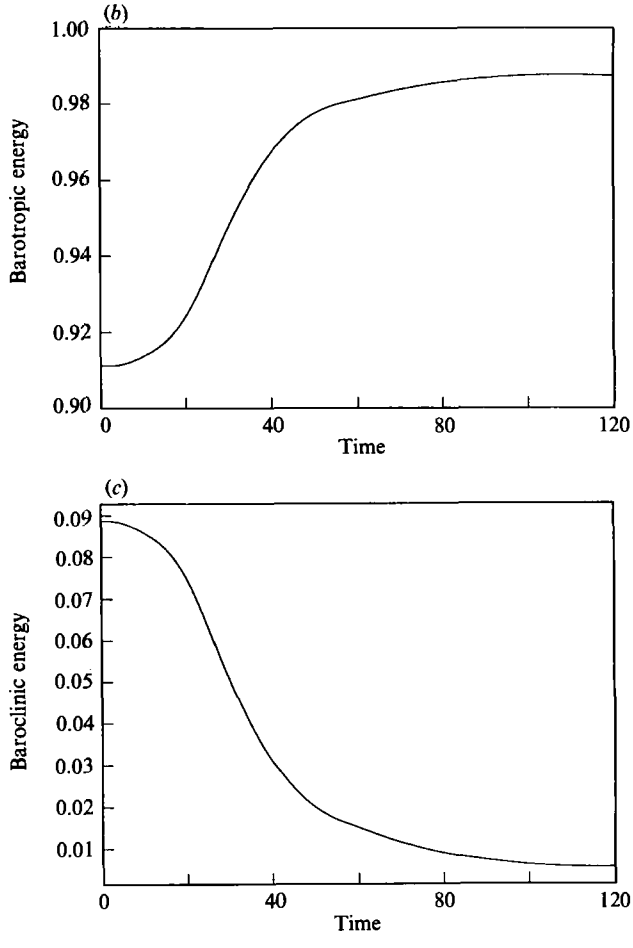

FIGURE 8. (*a*) The geostrophic potential vorticity fields for the alignment at $d_c = 3.0$ and $\gamma = 2.0$. The left (respectively right) column shows the lower (upper) layer. Compare this pseudospectral 128×128 computation with the contour surgery one in figure 1 (*a*) (the times of the spectral runs have to be rescaled by a factor of 4). (*b*) The barotropic energy *vs.* time for the run in (*a*). The units are chosen so that the total energy $E = E_T + E_C \equiv 1$ at $t = 0$. (*c*) The baroclinic energy *vs.* time for the run in (*a*). Same units as in (*b*).

parameter values are the same as the case presented in figure 1 (*a*), and it is easily seen that the results are very similar: the initially circular geostrophic potential vorticity patch in each layer is split into two parts, yielding an aligned barotropic central vortex surrounded by two satellite vortices (one in each layer). Since in figure 8 we have disposed the upper- and lower-layer fields next to each other, one can see directly that the intercentroid distance decreases as alignment takes place.

The barotropic and baroclinic energies (normalized by the total energy at $t = 0$) are shown in figures 8 (*b*) and 8 (*c*), respectively. The baroclinic energy E_C, initially approximately 9% of the total energy, decreases to less than 1% during alignment. At the same time, the barotropic energy E_T increases by acquiring the amount lost from E_C. Notice also how most of the energy conversion from E_C to E_T takes place between $t = 20$ and $t = 60$, which corresponds to the time when the vortices split into two pieces.

In contrast, the non-alignment case $d_c = 3.0$ and $\gamma = 1.0$ is shown in figure 9 (*a*)

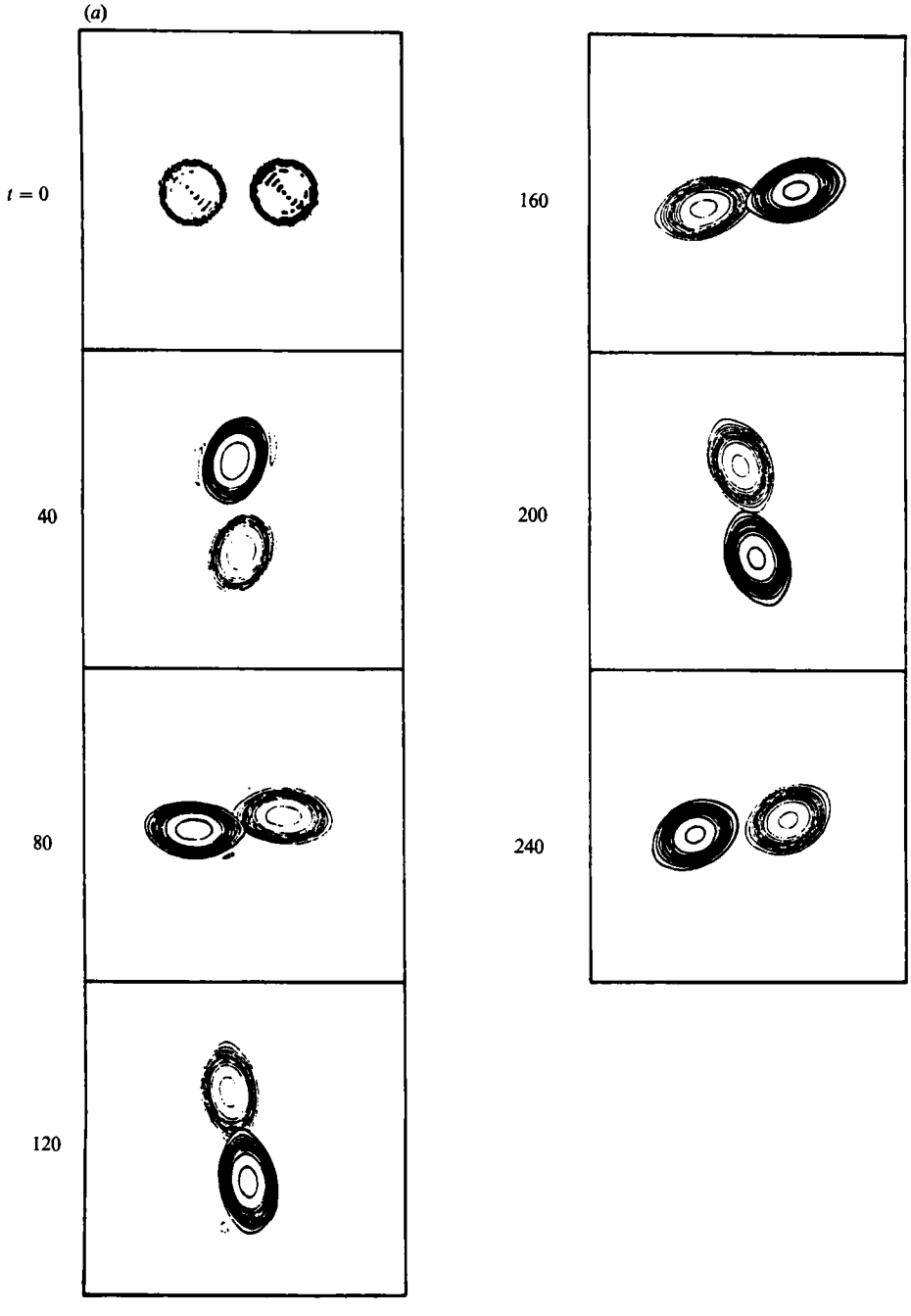

FIGURE 9(a). For caption see facing page.

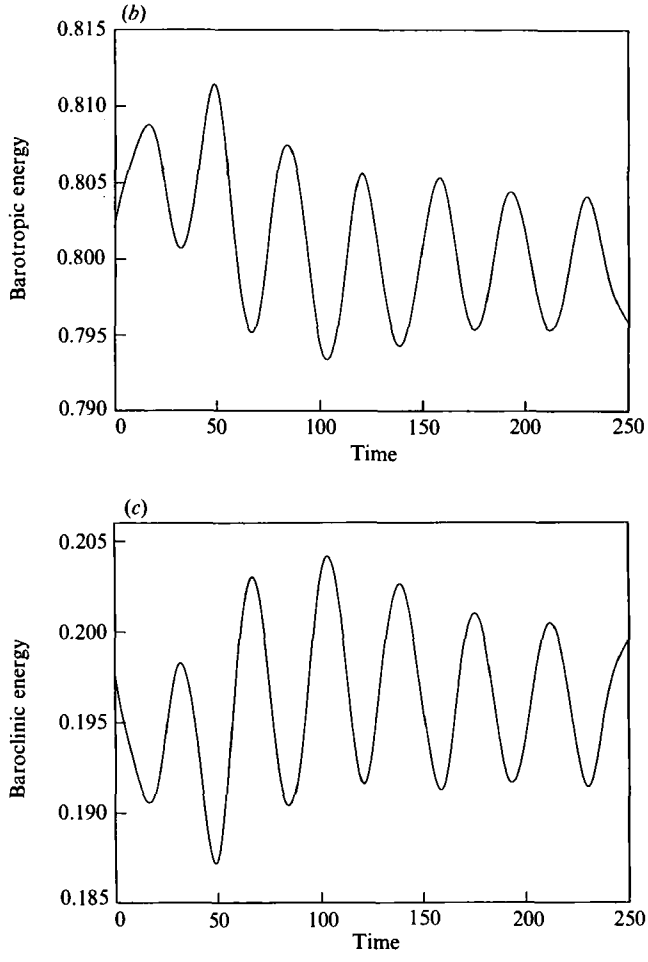

FIGURE 9. (*a*) Same as figure 8(*a*) but for $\gamma = 1.0$. Here the two layers have been superimposed; the darker (respectively lighter) vortex is in the upper (lower) layer. Compare this with the contour surgery run of figure 2(*a*). (*b*) The barotropic energy *vs.* time for the run in (*a*). The units are chosen so that the total energy $E = E_T + E_C \equiv 1$ at $t = 0$. (*c*) The baroclinic energy *vs.* time for the run in (*a*). Same units as in (*b*).

(this case can be compared with the contour surgery run of figure 2*a*). The energy partition (see figure 9*b*, *c*), approximately 20% baroclinic and 80% barotropic, only oscillates by less than 5% compared to the initial value. Note moreover that E_T and E_C are out of phase by precisely π, so that the oscillations represent an exchange between the barotropic and baroclinic modes. However, as opposed to the previous run, E_T and E_C retain – on average – their initial values.

4. Alignment and doubly connected rotating two-layer V-states

We now turn our attention to figure 7 and to the question of understanding the shape of the region where alignment occurs in the (γ, d_c) parameter space. As is the case for the merger problem (cf. the first paper), we intend to show that the shape of the alignment region is basically determined by the existence of V-states or, rather, the absence thereof. In other words, we wish to show that alignment takes place in that region in the (γ, d_c)-plane where stable V-states do not exist. We use the

term 'V-state' to describe any set of uniform geostrophic potential vorticity patches that rotate or translate at constant velocity without change in shape.

We have thus computed equilibria composed of two identical regions of uniform geostrophic potential vorticity, one in each layer, rotating about the origin with constant angular velocity Ω and with their centroids located symmetrically on either side of the origin on the x-axis. We designate these equilibria 'doubly connected two-layer rotating V-states' and a sketch of the geostrophic potential vorticity distribution associated with them is provided in figure 10. The algorithm used to determine these solutions is identical to the one described in the first paper, with the exception of the form for the Green function. All the V-states presented below were computed with 200 nodes on each vortex.

A lengthscale can be chosen without loss of generality (we choose it such that $x_B = 1$, see figure 10), and thus only one geometrical parameter is necessary to describe each V-state, namely the ratio $\nu \equiv x_A/x_B$. Being in different layers, the two vortices can overlap, in which case ν becomes negative. The range of interest is $-1 < \nu < 1$. The only other free parameter is γ. The way to proceed in finding V-states in this (ν, γ) parameter space is suggested by the shape of the curve in figure 7.

The question we wish to address is the following: for what values of ν and γ can doubly connected rotating V-states be found? Recall that when both vortices are in the same layer a V-state exists for any value of γ and $\nu > 0$, but the 'interesting' V-states (i.e. the ones relevant to the merger problem) are the ones for which $\nu = 0$. These are usually called 'limiting V-states', and correspond to the case when the two vortices are actually touching at the origin.

When the vortices are in different layers, however, the meaning of 'limiting V-state' needs to be understood in the original sense of Wu, Overman & Zabusky (1984). Namely, suppose that we are varying some parameter α and, having found a V-state at $\alpha = \alpha_0$, we find V-states for increasing values of $\alpha > \alpha_0$ up to $\alpha = \alpha_L$. If no V-state exists for $\alpha > \alpha_L$, we designate the V-state at $\alpha = \alpha_L$ as the 'limiting V-state'. For two-dimensional problems the parameter that indicates the existence of a limiting state is usually a geometrical one. Thus, for instance, the limiting V-state for doubly connected Euler (i.e. $\gamma = 0$ and $\Pi_2 = 0$) V-states occurs for $\nu_L = 0$.

The reason for this somewhat formal definition resides in the fact that, as we will show in what follows, for doubly connected rotating two-layer equilibria, limiting V-states occur in the parameter γ. The idea is simple: for a fixed value of the geometrical parameter ν, V-states always exist for sufficiently small γ but, when $\nu < 0$ (i.e. when the vortices have a non-vanishing overlap), there exists a value γ_L such that for $\gamma > \gamma_L$ the V-states cease to exist. A limiting V-state exists even when $\nu > 0$ (no overlap), but it is approached asymptotically as $\gamma \to \infty$.

The reason for proceeding by increasing γ at fixed ν in the exploration of the (ν, γ) parameter space is suggested by the single-valuedness of the curve for the critical alignment distance (cf. figure 7) when d_c is held fixed and γ is varied. Ideally, one would have liked to be able to calculate V-states at fixed d_c for increasing γ; however, our algorithm does not allow us to prescribe the value of d_c *a priori*. We can however hold ν fixed and, having found a V-state, compute the intercentroid distance d_1 and an equivalent radius R to construct the quantity $d_c = d_1/R$ which allows us to determine where the V-state is located in the (γ, d_c)-plane. (Since the vortices are not circular, the notion of radius is somewhat vague. We have adopted here the simplest definition: $R = (\text{Area}/\pi)^{\frac{1}{2}}$.)

We have proceeded as follows: for a fixed value of ν we have found doubly connected V-states by successively increasing γ from zero, until beyond $\gamma = \gamma_c$ our

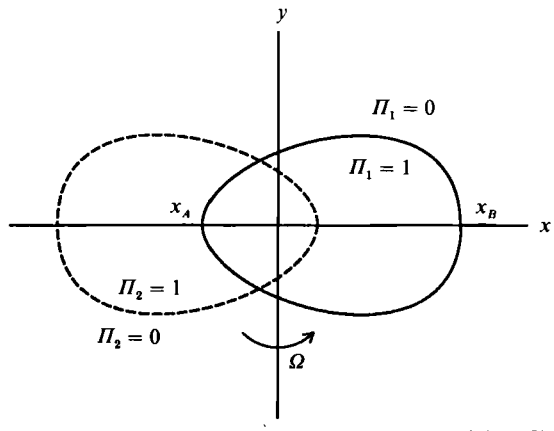

FIGURE 10. Schematic drawing of the geostrophic potential vorticity distribution of a doubly connected two-layer V-state. The solid (respectively dashed) vortex is located in the upper (lower) layer. The parameter ν is defined by $\nu \equiv x_A/x_B$.

ν	γ_c	d_c
−0.10	4.02	3.23
−0.15	1.29	2.00 (*)
−0.20	1.48	2.50 (*)
−0.30	1.23	1.34
−0.40	1.30	0.85
−0.50	1.44	0.66
−0.60	1.63	0.46
−0.70	1.92	0.29
−0.80	2.45	0.16

TABLE 1. The numerically determined values of d_c and γ_c for the limiting doubly connected rotating two-layer V-states as a function of the geometrical parameter ν. The values of γ_c in this table have been rescaled by a factor of $(\text{Area}/\pi)^{\frac{1}{2}}$ to make them comparable with the values in figure 7 for vortices of area π, as explained in the first paper. The asterisks are explained in §5.

algorithm fails to converge. Whether the value γ_c at which the algorithm stops converging corresponds to the value γ_L at which the V-states cease to exist, is a rather delicate question that we postpone to the next section. Suffice it to say that, for most values of ν, the two are identical (and we will provide computational evidence for this). We then compute the value of d_c for the V-state at $\gamma = \gamma_c$; these values are tabulated in table 1. We have also plotted them in figure 11, together with the curve for the critical alignment distance from figure 7.

Although the agreement between the two curves is not as close as for the merger problem, there is little doubt that the location where doubly connected rotating V-states cease to exist is a good 'zeroth-order predictor' for the boundary beyond which alignment can be expected to occur. The hatched sector between the two curves designates a region where we have found V-states and also observed alignment to take place; the V-states in this region have very high curvatures on their contours and there is every reason to believe that they would be unstable (we refer the reader to the first paper for a discussion of this point for the merger problem, where a similar phenomenon is observed).

Finally a comment must be made on the lower part of the curves in figure 11, where a region appears in which alignment does not occur in spite of the absence of

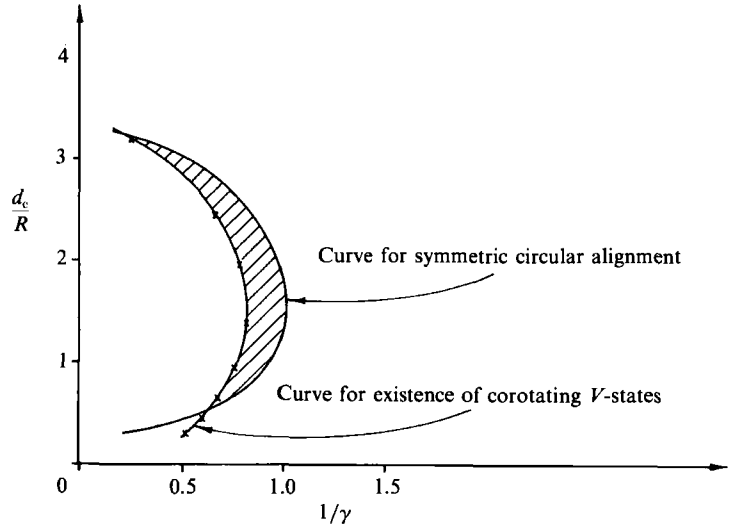

FIGURE 11. Alignment and existence of doubly connected two-layer rotating V-states. No V-states were found to the left of the curves, where alignment was observed to occur.

doubly connected rotating V-states. This may seem to invalidate our whole approach, but is easily explained if one considers the fact that for small values of d_c the initial condition is close to a second type of V-state, namely a barotropic vortex! Since this is stable to sufficiently small perturbations (Flierl 1988), no alignment is observed at small d_c.

5. Existence of V-states and corotating critical points

The next question to be addressed is why doubly connected rotating V-states cease to exist at a finite value of γ, as γ is progressively increased from zero at constant ν. To elucidate the matter we must proceed to a careful examination of the V-states themselves.

The $\nu > 0$ case is rather straightforward since the two vortices do not overlap. For $\gamma = 0$ the two layers are decoupled and the shape of the vortices is exactly circular. As γ is made non-zero, the vortices acquire a flattened shape, since they have to resist the shear induced by the vortex in the other layer and remain in equilibrium. In the limit $\gamma \to \infty$ the shapes of Euler doubly connected rotating V-states (previously studied by Saffman & Szeto 1980; Zabusky 1981; Dritschel 1985) are recovered, with the difference that Ω is scaled by a factor of $\frac{1}{2}$ with respect to the Euler value (this is because the two layers have equal depth; see the first paper for similar occurrences with other types of V-states).

An example of this type is presented in figure 12, where the doubly connected rotating two-layer V-states for $\nu = 0.1$ are plotted for several values of γ between 0.01 and 50. Several properties of these V-states are listed in table 2. As expected, the V-states at $\gamma = 10$, 20 and 50 are indistinguishable to the eye.

The situation becomes considerably more complicated when we allow the vortices to overlap. The V-states for the case $\nu = -0.1$ are shown in figure 13 and their properties presented in table 3. Notice that as γ is increased the V-states develop cusps in the region where the two vortices overlap, and eventually our algorithm fails to converge for $\gamma = \gamma_c \approx 11.90$.

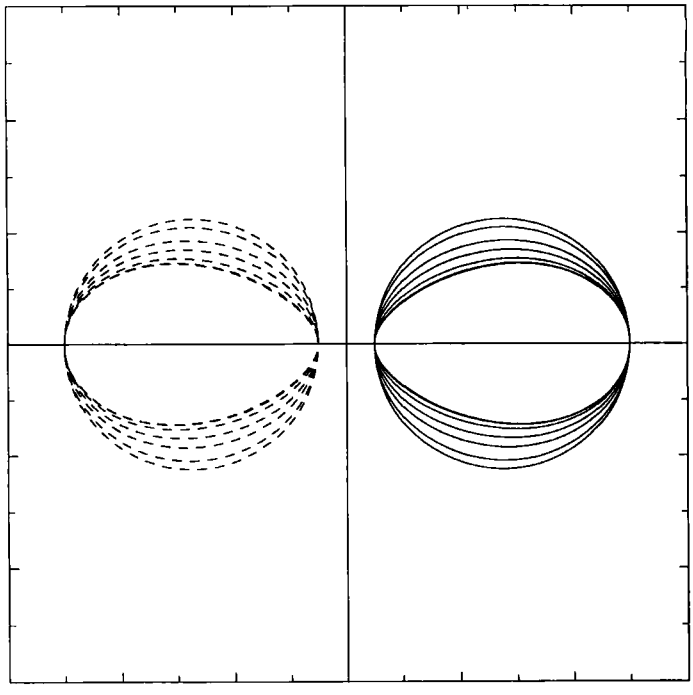

FIGURE 12. Doubly connected rotating two-layer V-states for $\nu = 0.1$. The values of γ for the V-states plotted here are given in table 2. The solid contours are in the upper layer, the dashed ones in the lower layer.

γ	Ω	d_1	λ	R	$\bar{x}$	Area
0.01	0.00005	2.445	1.000	0.450	0.550	0.636
1.00	0.04371	2.540	0.933	0.434	0.552	0.593
2.00	0.05820	2.717	0.826	0.408	0.555	0.524
3.00	0.05893	2.872	0.750	0.389	0.558	0.475
5.00	0.05556	3.054	0.677	0.369	0.563	0.427
10.00	0.05225	3.176	0.641	0.357	0.568	0.401
20.00	0.05147	3.201	0.636	0.355	0.569	0.397
50.00	0.05133	3.206	0.635	0.355	0.569	0.396

TABLE 2. Properties of doubly connected rotating two-layer V-states for $\nu = 0.1$. For each value of γ we tabulate the angular velocity Ω, the intercentroid distance d_1, the aspect ratio λ obtained by fitting the V-state to an ellipse with identical second-order moments, the equivalent radius $R \equiv (\text{Area}/\pi)^{\frac{1}{2}}$, the centroid $\bar{x}$ and the area of each vortex.

We have found that the most useful diagnostic for understanding these equilibria is an analysis of the geometry of the corotating stream function, i.e. the stream function in a frame of reference where the V-state is stationary. The corotating stream function is obtained from the stream function in the inertial frame by subtracting the term $\frac{1}{2}\Omega r^2$.

For a typical V-state in figure 13 far from the limiting one (i.e. at small γ), the geometry of the corotating stream function in the upper layer is sketched in figure 14. It goes without saying that the stream function in the lower layer is identical to the one in the upper layer upon reflection about the y-axis. Hence we need only discuss one of the two layers. The two centres C_1 and C_2 are a purely kinematic effect

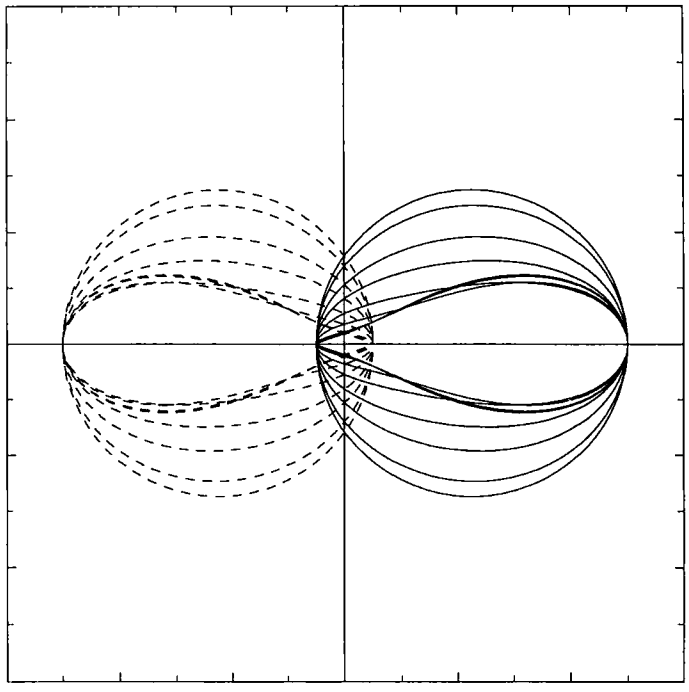

FIGURE 13. Doubly connected rotating two-layer V-states for $\nu = -0.1$. The values of γ for the V-states plotted here are given in table 3.

γ	Ω	d_1	λ	R	$\bar{x}$	Area
0.01	0.000 07	1.637	1.000	0.550	0.450	0.950
1.00	0.072 30	1.736	0.900	0.522	0.453	0.855
2.00	0.093 36	1.989	0.698	0.460	0.457	0.664
3.00	0.087 60	2.279	0.540	0.406	0.462	0.517
5.00	0.069 30	2.787	0.386	0.345	0.481	0.375
8.00	0.056 59	3.171	0.373	0.328	0.521	0.339
11.00	0.053 64	3.240	0.434	0.335	0.542	0.352
11.50	0.053 58	3.236	0.448	0.337	0.545	0.356
11.80	0.053 59	3.232	0.456	0.338	0.546	0.358
11.85	0.053 60	3.232	0.458	0.338	0.546	0.358
11.90	0.053 60	3.231	0.459	0.338	0.546	0.359

TABLE 3. Properties of the doubly connected rotating two-layer V-states for $\nu = -0.1$. (See the caption of table 2.) For this value of ν convergence stops at $\gamma_c = 11.90$.

due to the rotation of the frame of reference. They necessitate, however, the presence of the two saddle points S_1 and S_2. When $\gamma = 0$ the shape of the vortex is an exact circle and the geometry of figure 14 becomes degenerate (in that case the area enclosed by the separatrices vanishes, the four critical points C_1, C_2, S_1 and S_2 are located on a 'stagnation circle'). As γ is increased (at constant ν) the saddle point S_1 initially approaches the vortex contour, but is eventually pushed away from it until, at a special value $\gamma = \gamma_s$, the geometry of the corotating function undergoes a drastic topological change.

Beyond the threshold γ_s (for the case $\nu = -0.1$ we have found $\gamma_s \approx 4.5$) the influence in the upper layer of the vortex in the lower layer is so strong that it

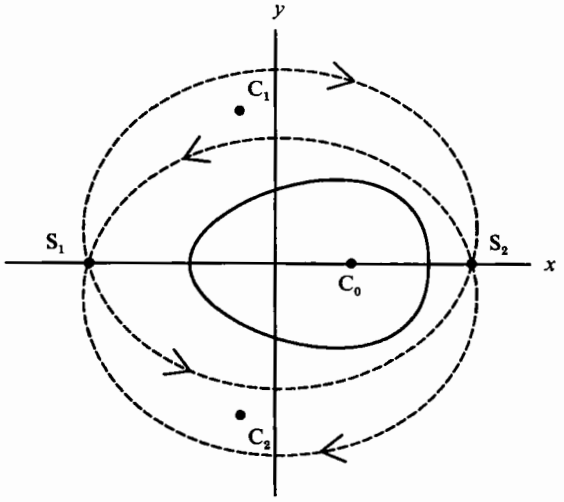

FIGURE 14. A sketch of the geometry of the corotating stream function in the upper layer for the doubly connected V-states of figure 13 at small γ. The solid line is the vortex boundary, the dashed lines the separatrices connecting the saddle points S_1 and S_2.

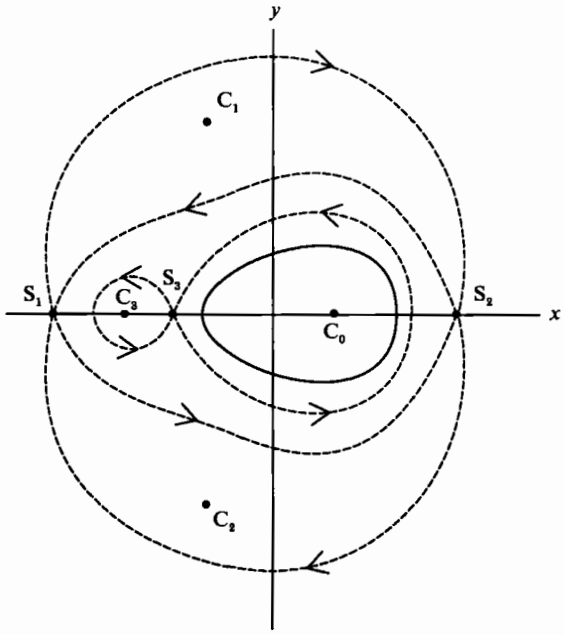

FIGURE 15. A sketch of the geometry of the corotating stream function in the upper layer for the doubly connected V-states of figure 13 at $\gamma > \gamma_s$. The closed streamlines around C_3 are due to the strong influence of the vortex in the lower layer.

generates a new set of closed contours in the upper layer, and therefore a new saddle and a new centre. A sketch of the associated corotating stream function, typical of V-states for $\gamma > \gamma_s$ is drawn in figure 15. The existence of a limiting V-state is a direct consequence of the presence of the saddle critical point S_3 which first appears as γ exceeds γ_s. As γ is further increased from γ_s, the size of the vortex centred in C_3 grows owing to the ever stronger effect of the vortex in the opposite layer. This pushes the

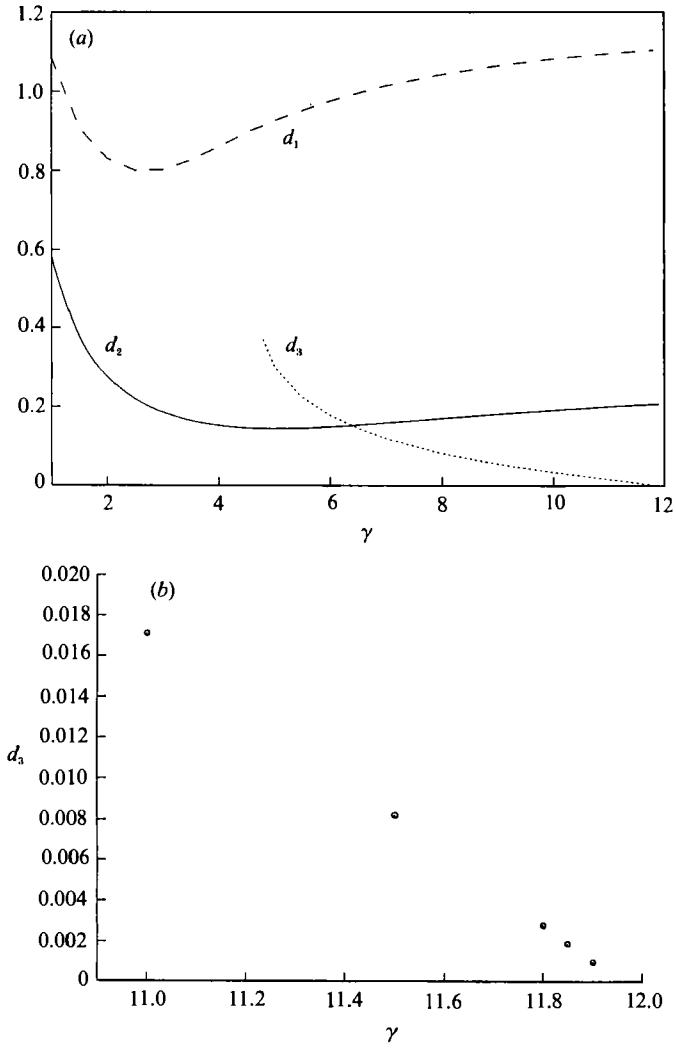

FIGURE 16. (*a*) The distances $d_k, k = 1, 2, 3$ along the x-axis between the boundary of the upper-layer vortex and the respective saddle stagnation points S_k as a function of γ for the V-states with $\nu = -0.1$ (cf. figure 13). Note that $d_3 \to 0$ near $\gamma = \gamma_c \approx 11.90$ where the limiting V-state is found. (*b*) An enlargement of (*a*) near γ_c, showing the intersection of d_3 with γ-axis near $11.90 < \gamma < 11.95$.

stagnation point S_3 closer and closer to the contour of the vortex patch until, at a finite value of $\gamma = \gamma_c$ the saddle point S_3 is on the contour itself and the limiting V-state is reached.

We have numerically computed the location of the stagnation points surrounding each V-state. The position (x_c, y_c) of each critical point is determined by solving (with a nonlinear secant method) the following two-dimensional system:

$$u_i(x_c, y_c) + \Omega x_c = 0, \quad v_i(x_c, y_c) - \Omega y_c = 0, \tag{5}$$

where u_i and v_i are the inertial velocities in layer i and are numerically evaluated by means of a contour integral over the known boundaries $\partial V_j\,(j = 1, 2)$ of the V-state:

$$[u_i, v_i](x, y) = -\frac{1}{2\pi} \sum_{j=1}^{2} \int_{\partial V_j} G_{ij}(r)\,[\mathrm{d}\xi, \mathrm{d}\eta], \tag{6}$$

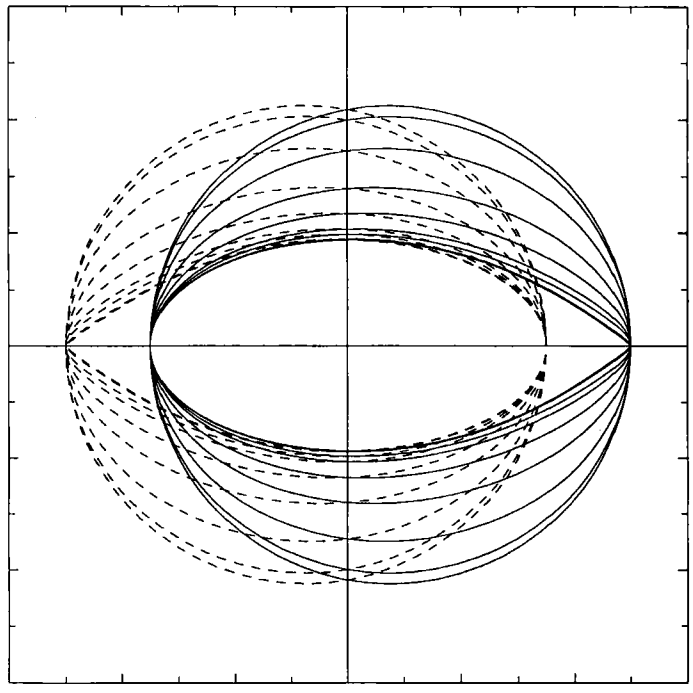

FIGURE 17. Doubly connected rotating two-layer V-states for $\nu = -0.7$. The values of γ for the V-states plotted here are given in table 4.

with $r^2 = (x-\xi)^2 + (y-\eta)^2$ and the Green functions G_{ij} given in the first paper (cf. equation (4)). Solution of (5) yields the location both centres and saddles, and we have found that convergence is very fast provided that the initial guess for the secant method is not too far from the critical point.

The results of our solution of (5) are presented in figure 16, where the numerical values of the distances d_k ($k = 1, 2, 3$) along the x-axis between the three stagnation points S_k and the boundary of the vortex are plotted versus γ. Note that the saddle point S_3, which appears for $\gamma > \gamma_s \approx 4.5$, touches the contour at finite $\gamma \approx 11.90$, while d_1 and d_2 actually grow at large γ and are always $O(1)$. An enlarged picture of the $11 < \gamma < 12$ region is given in figure 16*a*, showing the computational evidence for the existence of a limiting V-state near $\gamma \approx 11.90$.

The above scenario for the existence of a limiting V-state at finite γ applies, however, only to values of $0 > \nu > \tilde{\nu}$ for which the overlap between the two vortices is relatively small. (Our knowledge of the value of $\tilde{\nu}$ is somewhat crude since we have determined the V-states for only 10 distinct values of ν (cf. table 1); we find $-0.10 < \tilde{\nu} < -0.15$.) Beyond $\tilde{\nu}$ the situation is qualitatively different: the large overlap prevents the emergence of the closed contours centred around C_3 even when γ is large, and the geometry of the corotating stream function is similar to that shown in figure 14 for all values of γ. The limiting V-state in this case is due to the saddle point S_2 touching the contour at finite γ.

An example of this behaviour is illustrated in figure 17, where the V-states for $\nu = -0.7$ are plotted (see table 4 for their properties). In this case the cusps develop on the non-overlapping side of the vortices, and we find $\gamma_c \approx 3.55$. The distances of the critical saddle points S_1 and S_2 are plotted versus γ in figure 18(*a*), with an enlargement in figure 18(*b*) to show the limiting V-state at $\gamma_c \approx 3.55$. Note the

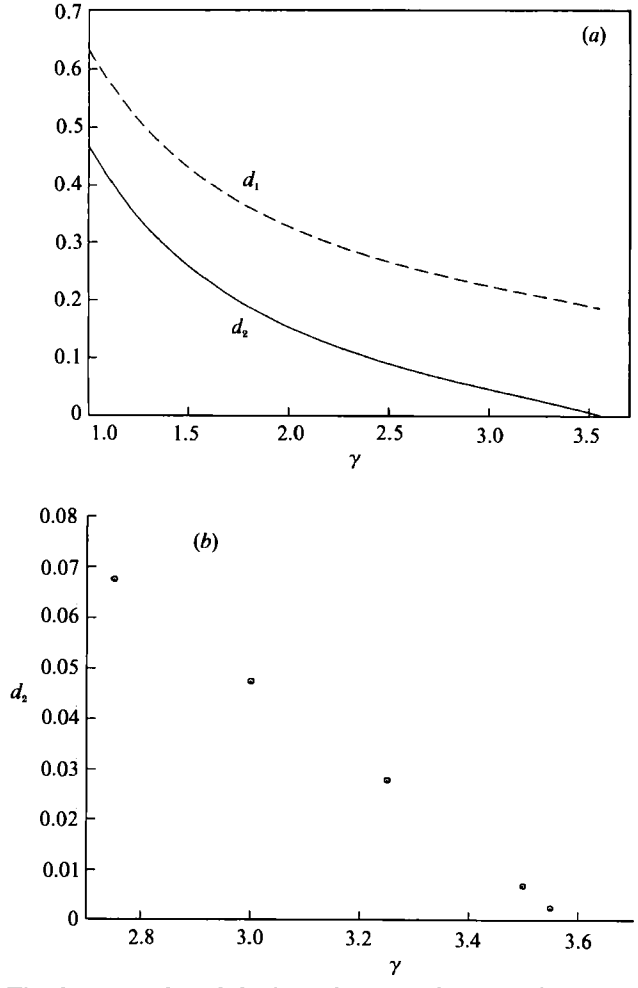

FIGURE 18. (*a*) The distances d_1 and d_2 along the x-axis between the boundary of the upper-layer vortex and the respective saddle stagnation points as a function of γ for the V-states with $\nu = -0.7$ (cf. figure 17). (*b*) An enlargement of (*a*) near γ_c, showing the intersection of d_2 with γ-axis near $3.5 < \gamma < 3.6$.

γ	Ω	d_1	λ	R	$\bar{x}$	Area
0.01	0.000 17	0.353	1.000	0.850	0.150	2.269
1.00	0.177 24	0.360	0.955	0.831	0.150	2.168
1.50	0.217 74	0.377	0.823	0.771	0.145	1.867
2.00	0.220 59	0.391	0.660	0.688	0.135	1.487
2.50	0.214 58	0.387	0.551	0.625	0.121	1.225
3.00	0.208 91	0.359	0.487	0.579	0.104	1.054
3.25	0.207 22	0.335	0.467	0.562	0.094	0.991
3.50	0.206 66	0.301	0.454	0.545	0.082	0.934
3.55	0.206 63	0.294	0.452	0.542	0.080	0.922

TABLE 4. Properties of the doubly connected rotating two-layer V-states for $\nu = -0.7$. (See the caption of table 2.) For this value of ν convergence stops at $\gamma_c = 3.55$.

monotonic character of the d_1 and d_2 curves in figure 18(*a*), in contrast with the richer behaviour at smaller values of ν (see figure 17).

For all but two values of ν (these are marked by asterisks in table 1) we have succeeded in showing that the point γ_c at which our algorithm fails to converge is associated with a critical saddle point touching the boundary, thereby establishing that γ_c is identical to γ_L, the point at which a limiting V-state exists. The failure of our algorithm to converge without a saddle point touching the contour is undoubtedly due to the weakness in our numerical scheme. The algorithm used here, based on the one of Wu *et al.* (1984), is only second order and is well known to have difficulties converging when cusps develop on the contours (see for instance Polvani & Carton 1989); a more powerful one (presumably of higher order, such as the one presented by Wu *et al.*) is probably necessary to converge on the limiting V-states at those two values of ν where the present scheme fails.

6. Finite-area hetons

As a final chapter in our investigation of the vortex dynamics of a two-layer system, we present in this section examples of translating V-states which are the finite-area analogues of the point-vortex pairs named 'hetons' by Hogg & Stommel (1985); they consist of two vortices of equal and opposite uniform geostrophic potential vorticity, located symmetrically about the y-axis, one in each layer, and translating with constant angular velocity V, as sketched in figure 19. The free geometrical parameter in this problem is the ratio $\mu \equiv x_A/x_B$.

Two-layer dipoles have been seen to emerge spontaneously from baroclinic instability by Helfrich & Send (1988), who showed how a baroclinic circular vortex perturbed with an unstable normal mode of angular wavenumber m breaks up into m finite-area hetons. Experimentally, Griffiths & Hopfinger (1986) have generated two-layer dipoles in their laboratory experiments and have studied their interactions.

We present next some of the translating dipolar two-layer V-states that we have determined with the same algorithm as used throughout this study. As for the V-states of the previous section, we have found that the situation becomes rather complicated when the two vortices have a large overlap and γ is large. For the sake of brevity, we will limit ourselves here to giving two simple examples.

When the two vortices do not overlap, i.e. for $\mu > 0$, the situation is similar to the one of the previous section. At $\gamma = 0$ the vortices are circular, they become more and more elongated as γ is increased and in the limit $\gamma \to \infty$ they converge to the same shape as the translating V-states of Deem & Zabusky (1978). The case $\mu = 0.05$ is shown in figure 20, and the properties of these V-states are presented in table 5.

It is easy to show that for a point-vortex heton of strength Γ and distance d_i between the two vortices, the propagation velocity is given by the formula

$$V_{pv} = \left(\frac{\Gamma}{2\pi}\right)\left[\frac{1}{d_i} - \sqrt{2\gamma} K_1(\sqrt{2\gamma} d_i)\right]. \tag{7}$$

However, we should warn the reader that the comparison between the velocity V of a finite-area heton and the equivalent point-vortex heton velocity V_{pv} with $\Gamma =$ Area is of little value unless γ is small. Indeed, while for a two-dimensional circular vortex of radius 1 the exterior field is identical to that of a point vortex of strength π (without loss of generality we take the vorticity to have value 1 throughout this discussion), such is not the case when the Green function is of modified Bessel type. Thus, for instance, it is easy to show that the strength s_{eq} of a point vortex that

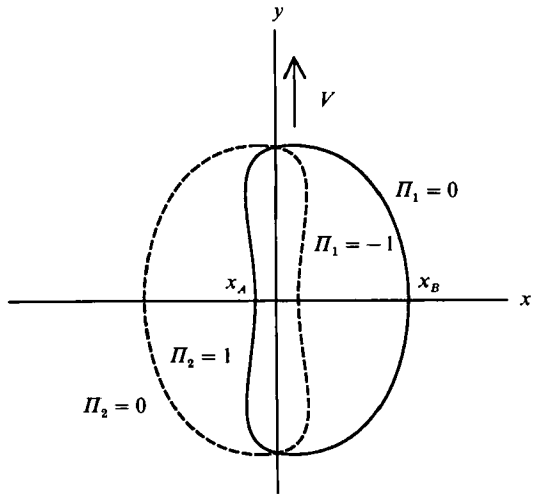

FIGURE 19. Schematic drawing of the geostrophic potential vorticity distribution of a finite-area heton. The solid (respectively dashed) vortex is located in the upper (lower) layer. The parameter μ is defined by $\mu \equiv x_A/x_B$.

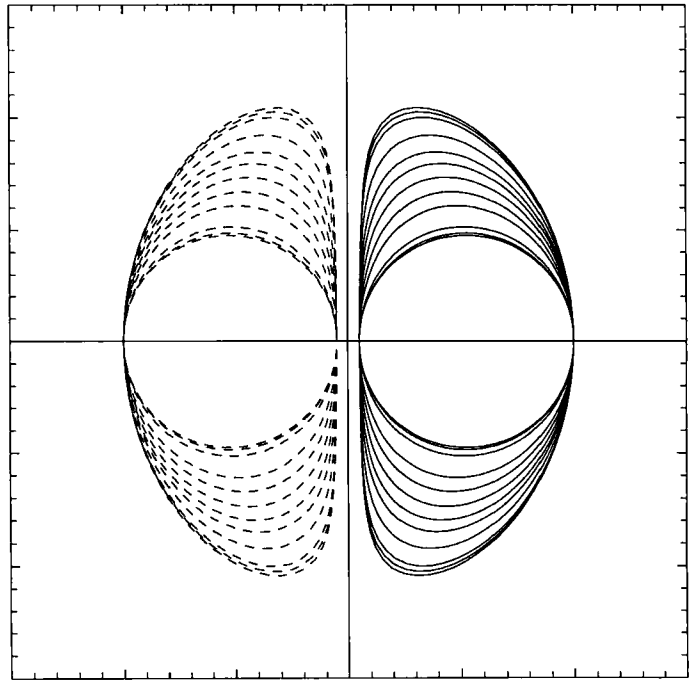

FIGURE 20. Two-layer dipoles for $\mu = 0.05$. The values of γ for these V-states are given in table 5.

produces a field identical to the exterior one of an equivalent barotropic circular vortex of radius 1 is given by

$$s_{\text{eq}} = \pi\left(\frac{2I_1(\gamma)}{\gamma}\right).$$

This, of course, reduces to π in the limit $\gamma \to 0$.

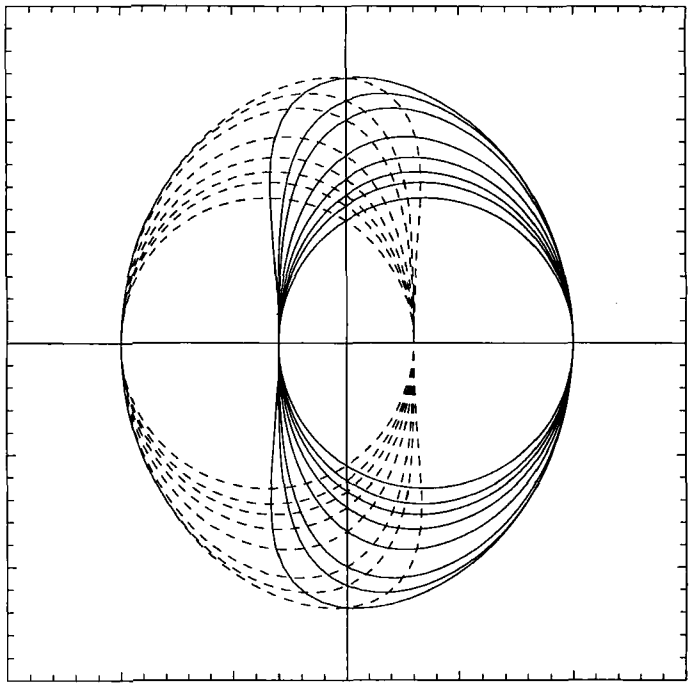

FIGURE 21. Two-layer dipoles for $\mu = -0.3$. The value of γ for these V-states are given in table 6.

γ	V	V/V_{pv}	Area	Area/A_0	d_i	λ	R
0.01	0.00003	0.979	0.709	1.000	1.050	0.999	0.475
0.50	0.01446	0.926	0.725	1.022	1.049	0.978	0.480
1.00	0.03051	0.904	0.768	1.084	1.045	0.924	0.494
2.00	0.05406	0.875	0.918	1.295	1.028	0.777	0.541
2.50	0.06329	0.856	1.017	1.435	1.015	0.704	0.569
3.00	0.07125	0.834	1.121	1.581	1.002	0.641	0.597
3.50	0.07779	0.812	1.218	1.719	0.990	0.591	0.623
4.00	0.08285	0.794	1.301	1.835	0.980	0.554	0.643
5.00	0.08932	0.770	1.415	1.996	0.967	0.508	0.671
7.50	0.09535	0.747	1.530	2.159	0.954	0.468	0.698
10.00	0.09704	0.741	1.565	2.208	0.951	0.456	0.706
50.00	0.09825	0.735	1.591	2.244	0.948	0.448	0.712

TABLE 5. Properties of finite-area hetons for $\mu = 0.05$. For each value of γ we tabulate the velocity V, its ratio the velocity of the equivalent point-vortex heton V_{pv}, the area of each vortex and its ratio to the area A_0 at $\gamma = 0$, the intercentroid distance d_i, the aspect ratio λ obtained by fitting each vortex to an ellipse with identical second-order moments and the equivalent radius $R \equiv (\text{Area}/\pi)^{\frac{1}{2}}$.

As a final example we show in figure 21 the finite-area hetons for $\mu = -0.3$ (see table 6 for their properties). When the overlap is considerable the vortices tend to look 'bean shaped'. The largest value of γ for which the algorithm converged is $\gamma = 2.20$. We have also obtained solutions at larger values of negative μ (greater overlap) but their shapes are more difficult to understand. We are currently in the process of analysing them and we hope to report on that in the future.

γ	V	V/V_{pv}	Area	Area/A_0	d_i	λ	R
0.01	0.00004	0.925	1.327	1.000	0.700	0.999	0.650
1.00	0.04405	0.670	1.470	1.108	0.692	0.903	0.684
1.25	0.05535	0.630	1.568	1.181	0.685	0.847	0.706
1.50	0.06627	0.586	1.707	1.286	0.674	0.780	0.737
1.75	0.07694	0.535	1.905	1.435	0.655	0.702	0.779
2.00	0.08684	0.468	2.196	1.654	0.620	0.615	0.836
2.10	0.08979	0.430	2.354	1.774	0.594	0.577	0.866
2.20	0.08805	0.364	2.562	1.930	0.530	0.536	0.903

TABLE 6. Properties of finite-area hetons for $\mu = -0.3$. (See the caption of table 5.) Convergence was lost at $\gamma \approx 2.2$.

7. Summary and conclusions

The purpose of this study has been to investigate the vortex dynamics of a very simple physical system (the quasi-geostrophic two-layer model) that, although retaining many of the simplifications of two-dimensional flows, allows for vertical variations characteristic of the rapidly rotating stratified flows found in planetary atmospheres. The question of vortex coalescence has occupied a prominent place in this study, since it is the fundamental process leading to the formation of the strong isolated coherent structures observed in turbulence simulations.

We have examined in detail the two simplest cases of coalescence, where two circular uniform geostrophic potential vorticity regions interact in the same layer (merger) or from different layers (alignment). We have studied the dependence of these two processes on the radius of deformation of the system and the initial distance between the two vortices.

One of the major findings of this work is that the behaviour of a given configuration of geostrophic potential vorticity depends crucially on its proximity to a stable equilibrium state: if it is 'far' from any equilibrium, it has to rearrange itself considerably (through repeated filamentation) before it becomes close to a V-state. Hence the occurrence of merger and alignment, which are essentially inviscid processes in the early stages, depends on where V-states are found; where no stable doubly connected equilibrium exists, the vorticity rearranges itself to the 'closest' available equilibrium, often, but not always, an axisymmetric configuration. Figure 22 shows a blow-up of the frame $t = 11$ of the alignment on figure 3(*a*); the shapes of the two central vortices are remarkably close to the V-states shown on figure 17. Note that the same shapes reappear periodically (see frames $t = 18$ and $t = 25$), in spite of the presence of vorticity filaments.

The analysis of the comoving stream function, its geometry and, in particular, the location of the hyperbolic critical points, which have been known to play an essential role in the *dynamical* evolution of vorticity fields†, have here been shown to yield much insight into *static* problems as well, more specifically in determining the existence of V-states.

In many ways, we consider this study to be only a partial investigation of a very rich subject, with many questions still in need of an answer. Perhaps the greatest limitation of this work is the representation of geostrophic vortices as uniform

† For the problems of axisymmetrization and merger see Melander, McWilliams & Zabusky (1987) and Melander, Zabusky & McWilliams (1988), respectively, and for the filamentation problem see Polvani *et al.* (1989*b*) and Pullin *et al.* (1989).

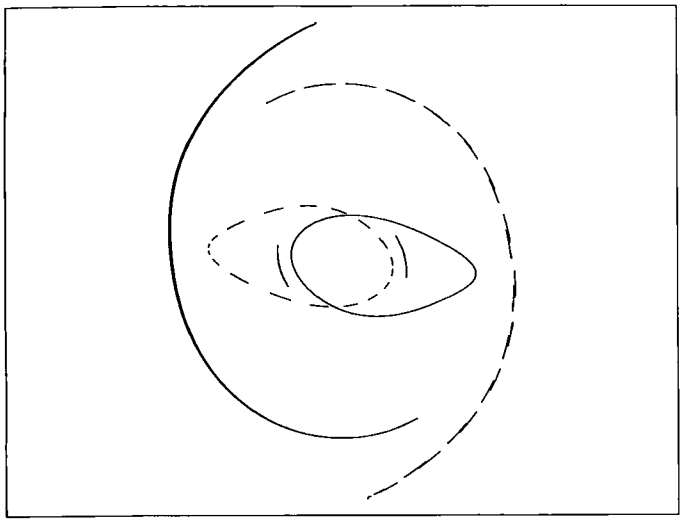

FIGURE 22. An enlargement of the frame $t = 11$ of figure 3(*a*). Compare the vortex shapes with the V-states shown in figure 17.

potential vorticity patches. As Verron, Hopfinger & McWilliams (1990) have recently shown for the merger problem, representing vortices as regions of anomalous relative vorticity leads to quite different results to those obtained in this study. Another limitation of this work is the fact that the stratification was represented by only two density layers. The question of alignment in the presence of a continuous stratification, for instance, would be considerably richer, since vortices can coalesce from non-contiguous density levels. All in all much work remains to be done to advance our understanding of coherent vortex structures in geostrophic turbulence.

The author wishes to thank Glenn Flierl, Norman Zabusky and Jim McWilliams for useful suggestions and discussions, David Dritschel for providing the one-layer contour surgery code and Xavier Carton for helping with the pseudospectral computations. This research was supported, in part, by the Office of Naval Research, under grant N00014-86-K-0325.

REFERENCES

BABIANO, A., BASDEVANT, C., LEGRAS, B. & SADOURNY, R. 1986 Vorticity and passive scalar dynamics in two-dimensional turbulence. *J. Fluid Mech.* **183**, 379–397.

BENZI, R., PATERNELLO, S. & SANTANGELO, P. 1988 Self-similar coherent structures in two-dimensional decaying turbulence. *J. Phys* A **21**, 1221–1237.

CHARNEY, J. C. 1971 Geostrophic turbulence. *J. Atmos. Sci.* **28**, 1087–1095.

DEEM, G. S. & ZABUSKY, N. J. 1978 Stationary V-states: interactions, recurrence and breaking. *Phys. Rev. Lett.* **40**, 859.

DRITSCHEL, D. G. 1985 The stability and energetics of corotating uniform vortices. *J. Fluid Mech.* **157**, 95–134.

DRITSCHEL, D. G. 1988*a* Contour surgery: a contour dynamics method for long time behavior of two-dimensional, inviscid, rotational flow. *J. Comput. Phys.* **77**, 240–266.

DRITSCHEL, D. G. 1988*b* The repeated filamentation of two-dimensional vorticity interfaces. *J. Fluid Mech.* **194**, 511–532.

FLIERL, G. R. 1988 On the instability of geostrophic vortices. *J. Fluid Mech.* **197**, 349–388.

FLIERL, G. R., LARICHEV, V. D., MCWILLIAMS, J. C. & REZNIK, G. M. 1980 The dynamics of baroclinic and barotropic solitary eddies. *Dyn. Atmos. Ocean* **5**, 1–41.

GRIFFITHS, R. W. & HOPFINGER, E. J. 1986 Experiments with baroclinic vortex pairs in a rotating fluid. *J. Fluid Mech.* **173**, 501–518.

GRYANICK, V. M. 1983 Dynamics of singular geostrophic vortices in a two-level model of the atmosphere (or the ocean). *Izv. Acad. Nauk SSSR Atmos. Ocean. Phys.* **19**, 171–179.

HELFRICH, K. & SEND, U. 1988 Finite amplitude evolution of two-layer geostrophic vortices. *J. Fluid Mech.* **197**, 331–348.

HERRING, J. R. 1980 Statistical theory of quasigeostrophic turbulence. *J. Atmos. Sci.* **37**, 969–977.

HOGG, N. & STOMMEL, H. 1985 The heton, an elementary interaction between discrete baroclinic geostrophic vortices and its implication concerning eddy heat-flow. *Proc. R. Soc. Lond.* A **397**, 1–20.

HUA, L. B. & HAIDVOGEL, D. B. 1986 Numerical simulation of the vertical structure of quasigeostrophic turbulence. *J. Atmos. Sci.* **43**, 2923–2936.

KRAICHNAN, R. H. & MONTGOMERY, D. 1980 Two-dimensional turbulence. *Rep. Prog. Phys.* **43**, 547–619.

MCWILLIAMS, J. C. 1984 The emergence of isolated coherent vortices in turbulent flow. *J. Fluid Mech.* **146**, 21–43.

MCWILLIAMS, J. C. 1989 Statistical properties of decaying geostrophic turbulence. *J. Fluid Mech.* **198**, 199–230.

MELANDER, M. V., MCWILLIAMS, J. C. & ZABUSKY, N. J. 1987 Axisymmetrization and vorticity gradient intensification of an isolated two-dimensional vortex through filamentation. *J. Fluid Mech.* **178**, 137–159.

MELANDER, M. V., ZABUSKY, N. J. & MCWILLIAMS, J. C. 1988 Symmetric vortex merger in two dimensions: causes and conditions. *J. Fluid Mech.* **195**, 303–340.

POLVANI, L. M. 1988 Geostrophic vortex dynamics. Ph.D. thesis, Massachusetts Institute of Technology and Woods Hole Oceanographic Institution, WHOI-88-48.

POLVANI, L. M. & CARTON, X. J. 1989 The tripole: a new coherent vortex structure of incompressible two-dimensional flows. *Geophys. Astrophys. Fluid Dyn.* **51**, 87–102.

POLVANI, L. M., FLIERL, G. R. & ZABUSKY, N. J. 1989*b* Filamentation of coherent vortex structures via separatrix crossing: a quantitative estimate of onset time. *Phys. Fluids* A **1**, 181–184.

POLVANI, L. M., ZABUSKY, N. J. & FLIERL, G. R. 1989*a* Two-layer geostrophic vortex dynamics. Part 1. Upper-layer V-states and merger. *J. Fluid Mech.* **205**, 215–242.

PULLIN, D. I., JACOBS, P. A., GRIMSHAW, R. H. J. & SAFFMAN, P. G. 1989 Stability and filamentation of finite-amplitude waves on vortex layers of finite thickness. *J. Fluid Mech.* **209**, 359–384.

RHINES, P. B. 1979 Geostrophic turbulence. *Ann. Rev. Fluid Mech.* **11**, 401–441.

SAFFMAN, P. G. & SZETO, R. 1979 Equilibrium shapes of a pair equal uniform vortices. *Phys. Fluids* **23**, 171–185.

VERRON, J., HOPFINGER, E. J. & MCWILLIAMS, J. C. 1990 Sensitivity to initial conditions in the merging of two-layer baroclinic vortices. *Phys. Fluids* A **2**, 886–889.

WU, H. M., OVERMAN, E. A. & ZABUSKY, N. J. 1984 Steady state solutions of the Euler equations in two dimensions. Rotating and translating V-states with limiting cases. I. Numerical algorithms and results. *J. Comput. Phys.* **53**, 42–71.

ZABUSKY, N. J. 1981 Recent developments in contour dynamics for the Euler equations. *Ann. NY Acad. Sci.* **373**, 160–170.